*Steel and Composite Structures, Vol. 14, No. 1 (2013) 1-20*
DOI: http://dx.doi.org/10.12989/scs.2013.14.1.001


# Nonlinear *P*-Δ analysis of steel frames with semi-rigid connections

Hamid R. Valipour*[1] and Mark A. Bradford[2]

[1]*Centre for Infrastructure Engineering and Safety, School of Civil and Environmental Engineering, The University of New South Wales*
[2]*Centre for Infrastructure Engineering and Safety, The University of New South Wales*

*(Received July 29, 2010, Revised July 26, 2012, Accepted November 13, 2012)*

**Abstract.** This paper presents the formulation for a novel force-based 1-D compound-element that captures both material and second order *P*-Δ nonlinearities in steel frames. At the nodal points, the element is attached to nonlinear rotational and a translational springs which represent the flexural and axial stiffness of the connections respectively. By decomposing the total strain in the material as well as the generalised displacements of the flexible connections to their elastic and inelastic components, a secant solution strategy based on a direct iterative scheme is introduced and the corresponding solution strategy is outlined. The strain and slope of the deformed element are assumed to be small; however the equilibrium equations are satisfied for the deformed element taking account of *P*-Δ effects. The formulation accuracy and efficiency is verified by some numerical examples on the nonlinear static, cyclic and dynamic analysis of steel frames.

**Keywords:** flexibility; nonlinearity; *P*-Δ effects; secant stiffness; semi-rigid connection

## 1. Introduction

The conventional analysis and design of steel structures considers the behaviour of the beam-to-column connections as being either rigid-joints or pinned-joints. In reality, however, it is well-known that most connections are neither fully rigid nor perfectly pinned, and they exhibit semi-rigid deformation behaviour which can significantly contribute to the overall frame deflection and they also affect the distribution of internal forces in the connected members (Trahair *et al*. 2008).

Over the last thirty years, extensive research has been devoted to numerical and experimental studies and to the practical design of steel and steel-composite frames with semi-rigid connections (Stelmack *et al*. 1986, Chen *et al*. 1996, Rodrigues *et al*. 1998, Ivanyi 2000, Ashraf *et al*. 2004, da S. Vellasco *et al*. 2006, Wang and Li 2007, Liu *et al*. 2008, Wang and Li 2008, de Lima *et al*. 2009, Hadianfard 2012, Reyes-Salazar *et al*. 2012), and others. These studies cover various local and global aspects of semi-rigid steel frames, such as material, connection and geometrical nonlinearities (Cheng and Juang 1986, Liew *et al*. 1997, Sekulovic and Salatic 2001, Bayo *et al*. 2006, Chan and Cho 2008, Chiorean 2009), the response of semi-rigid connections (Chen and Kishi 1989, Kishi and Chen 1990, Attiogbe and Morris 1991, Shen and Astaneh-Asl 1999, Shi *et*

*Corresponding author, Ph.D., E-mail: H.Valipour@unsw.edu.au

*al*. 2008), the effects of elevated temperature and fire on the global response as well as the local behaviour of connections (Spyrou *et al*. 2004, Han *et al*. 2007, Iu *et al*. 2007, Ding and Wang 2009) and the vibration and nonlinear dynamic analysis of semi-rigid steel frames subjected to extreme loads such as earthquake and blast (Cheng and Juang, 1986, Chui and Chan, 1996, da Silva *et al*. 2008, Khandelwal *et al*. 2008, Sekulovic and Nefovska-Danilovic 2008, Vu and Leon 2008, Saravanan *et al*. 2009, Zarfam and Mofid 2009).

The nonlinear continuum-based finite element models for frame components offer the good versatility and accuracy required for a detailed study of local effects, but they are computationally demanding and can be intractable in modelling frames with multiple beams and columns. 1-D frame elements, however, are a good compromise between accuracy and efficiency, which is required for capturing the global response of multi-storey multi-bay frames and is the focus of this paper (Chan and Chui 2000).

Nonlinear frame elements can be formulated in the framework of lumped models or of distributed nonlinearity models. These lumped models, which have been used extensively for the nonlinear analysis of semi-rigid steel and steel-composite frames offer superior efficiency (Bayo *et al*. 2006, Chiorean 2009, Iu *et al*. 2009), whereas distributed nonlinearity models which are the focus of this paper have superior accuracy and they do not need a priori knowledge of plastic hinge position and length. Further details on the classification of models along with their pros and cons can be found in Chan and Chui (2000).

In this paper, the concept of total strain (generalised displacement) decomposition to its elastic and inelastic components is adopted to derive the secant stiffness of sections and of nodal springs which represent the semi-rigid connections. Further, the exact force interpolation functions are employed to derive the element secant stiffness and a direct iteration scheme consistent with this secant formulation is presented. Geometrical nonlinearity is taken into account by satisfying the equilibrium equations for the deformed element ($P$-$\Delta$ effects); however, the strains and slope are assumed to be small. A composite Simpson integration scheme, accompanied with a parabolic piecewise interpolation of the curvature function, is used to establish the deformed shape of the element required for updating the geometry (Valipour and Foster, 2010b, Valipour and Bradford, 2012). The accuracy and efficiency of the formulation is verified by some numerical examples considering the nonlinear static, cyclic and dynamic analysis of steel frames.

## 2. Element formulation

### *2.1 Compatibility equations*

Adopting the Navier-Bernoulli assumptions, section compatibility requirements produce

$$\varepsilon_x = \varepsilon_r - y\kappa\,, \tag{1}$$

where $\varepsilon_x$ denotes the total strain at the integration point in the local $x$-$x$ direction (along the element axis; Fig 1(a)), $\varepsilon_r$ denotes the section axial strain, $\kappa$ denotes the total curvature of section and $y$ is the distance of the integration point (fibre) from the mid-plane of the element.

Fig. 1(a) shows a 2-node plane frame element $AB$ with three degrees of freedom at each node. Furthermore, at each nodal point the element is attached to a rotational and a translational spring which represent the flexural and axial stiffness of the connections respectively (Fig. 1(a)). The generalised nodal displacement and force vectors (with rigid body modes) are denoted by $q$ and

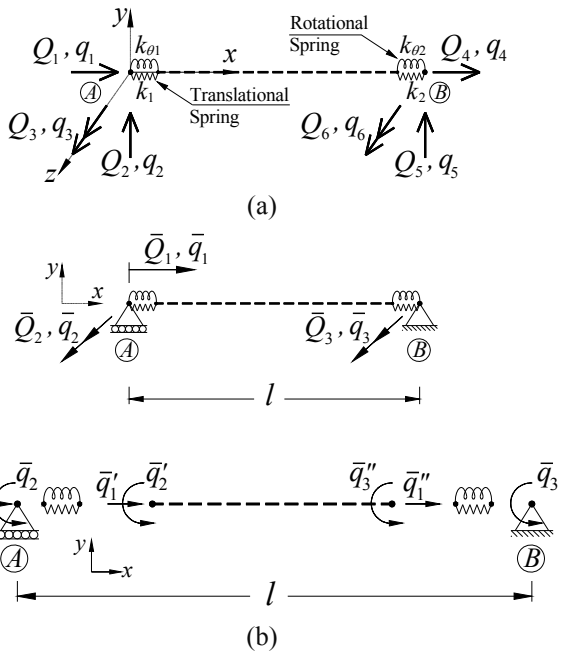


Fig. 1 (a) 2-node frame element *AB* in *x*-*y* plane (b) outline of the simply supported configuration (system without rigid body modes)

$Q$, respectively. Using the principle of virtual force for the simply supported configuration shown in Fig. 1(b), the strain-deformation compatibility equation for the frame element (without nodal springs) is obtained as

$$\overline{\mathbf{q}}' = \int_0^l \mathbf{b}^T(x)\, \mathbf{d}(x)\, dx \quad , \tag{2}$$

where

$$\mathbf{b}(x) = \begin{bmatrix} -1 & 0 & 0 \\ 0 & x/l - 1 & x/l \end{bmatrix} \quad , \tag{3}$$

$\overline{\mathbf{q}}' = \left[\bar{q}_1' - \bar{q}_1''\quad \bar{q}_2'\quad \bar{q}_3'\right]^T$ is the vector of the generalised nodal deformations excluding the nodal springs (without rigid body modes) and $\mathbf{d}(x) = \left[\varepsilon_r \quad \kappa\right]^T$ is the vector of the section generalised strains.

### *2.2 Equilibrium equations and constitutive material law*

The equilibrium of the deformed configuration *Ax* (Fig. 2) leads to the matrix representation

$$\overline{\mathbf{D}}(x) = \mathbf{b}(x)\,\overline{\mathbf{Q}} + \overline{\mathbf{D}}_{und.}(x)\,, \tag{4}$$

in which

$$\overline{\mathbf{D}}_{und.}(x) = \left[0 \quad Q_1 v'(x)\right]^T, \tag{5}$$

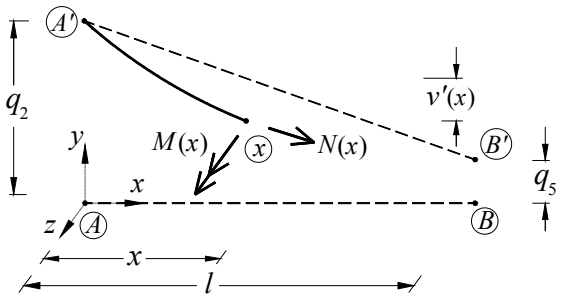


Fig. 2 Free body diagram of *Ax* after deformation

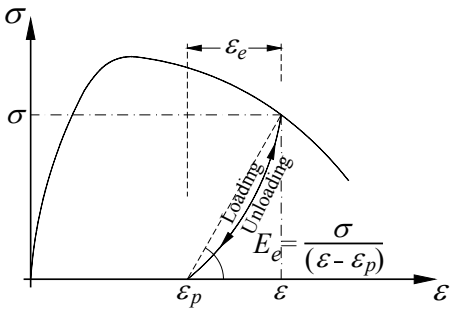


Fig. 3 Typical uniaxial stress-strain relationship in a total secant framework

$\overline{\mathbf{Q}} = \left[\overline{Q}_1 \quad \overline{Q}_2 \quad \overline{Q}_3\right]^T$ denotes the nodal force vector (in the system without rigid body modes), $\overline{\mathbf{D}}(x) = \left[N(x) \quad M(x)\right]^T$ is the section internal force vector and $\overline{\mathbf{D}}_{und.}(x)$ refers to undulation effect which represents the deflection of the element with respect to the rotated axis of the element after the deformation (Carol and Murcia 1989a).

Decomposing the total axial strain $\varepsilon_x$ into elastic $\varepsilon_{ex}$ and inelastic $\varepsilon_{px}$ components, and using the equations of equilibrium across the section (Valipour and Foster 2010a) gives

$$\overline{\mathbf{D}}(x) = {}^{e}\mathbf{k}_s(x)\, d(x) + \overline{\mathbf{D}}_p(x), \tag{6}$$

in which

$$\mathbf{k}_s(x) = \begin{bmatrix} \int_\Omega E_e\, dA & -\int_\Omega y\, E_e\, dA \\ -\int_\Omega y\, E_e\, dA & \int_\Omega y^2\, E_e\, dA \end{bmatrix}, \tag{7}$$

$$\overline{\mathbf{D}}_p(x) = \left[-\int_\Omega E_e . \varepsilon_{px}\, dA \quad \int_\Omega y\, E_e . \varepsilon_{px}\, dA\right]^T, \tag{8}$$

and where $y$ is the distance of the integration point from the element mid-plane, $E_e$ is the elastic secant modulus of the theoretical unloading curve (Fig. 3) and $\mathbf{k}_s(x)$ and $\overline{\mathbf{D}}_p(x)$ denote the secant stiffness matrix and the vector of residual plastic force, respectively.

The flexibility matrix of the section $\mathbf{f}_s(x)$ is obtained by inverting the section stiffness matrix, and then Eq. (6) can be rearranged as

$$\mathbf{d}(x) = \mathbf{f}_s(x)\, \left\{\overline{\mathbf{D}}(x) - \overline{\mathbf{D}}_p(x)\right\}. \tag{9}$$

Using Eqs. (4) and (9), the section generalised strain vector $\mathbf{d}(x)$ is related to $\overline{\mathbf{Q}}$, and then substituting the results into Eq. (2) gives the relationship

$$\overline{\mathbf{q}}' = \mathbf{F}\, \overline{\mathbf{Q}} + \overline{\mathbf{q}}_p + \overline{\mathbf{q}}_{und.}, \tag{10}$$

where

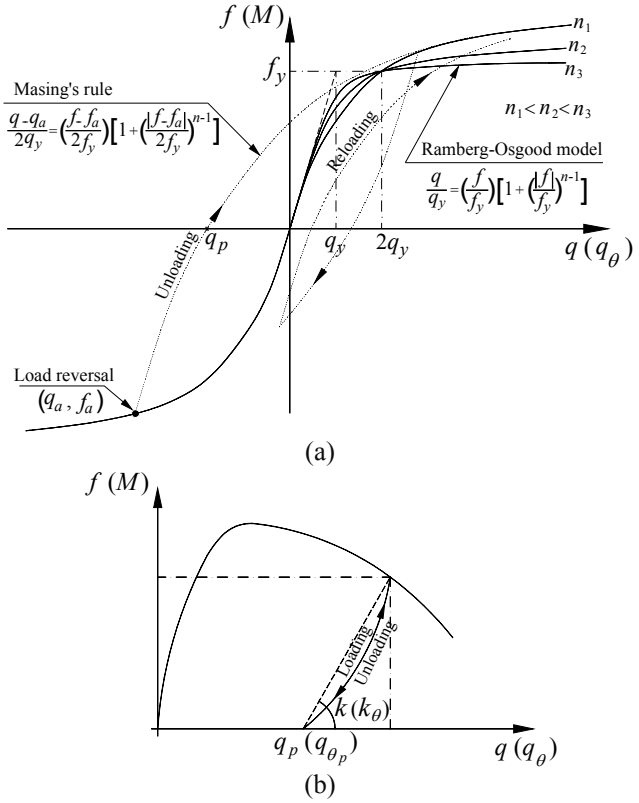


Fig. 4 (a) Ramberg-Osgood model for semi-rigid connections with Masing's rule for unloading/reloading branch (b) outline of the generalised force-displacement relationship for semi-rigid connections in the total secant framework

$$\mathbf{F} = \int_0^l \mathbf{b}^T(x)\ \mathbf{f}_s(x)\ \mathbf{b}(x)\ dx \tag{11}$$

is the flexibility matrix of the simply supported element (without rigid body modes),

$$\overline{\mathbf{q}}_p = -\int_0^l \mathbf{b}^T(x)\ \mathbf{f}_s(x)\ \overline{\mathbf{D}}_p(x)\,dx \tag{12}$$

is the nodal generalised plastic deformation vector excluding the nodal springs, and

$$\overline{\mathbf{q}}_{und.} = \int_0^l \mathbf{b}^T(x)\ \mathbf{f}_s(x)\ \overline{\mathbf{D}}_{und.}(x)\,dx \tag{13}$$

is the nodal generalised deformation vector due to the undulation effects.

### *2.3 Constitutive law for semi-rigid connections*

Adopting the compound-element concept, the rotational and horizontal stiffnesses of the semi-rigid connections are represented by assigning equivalent springs to the beam nodal points

(Fig. 1(b)). Behavioural models of semi-rigid connections have been the subject of numerous experimental and analytical studies in the published literature (Kukreti and Abolmaali 1999, Ivanyi 2000, Simoes Da Silva *et al*. 2004, Mohamadi-shooreh and Mofid 2008, Prabha *et al*. 2008), and various analytical expressions in the form of a piecewise linear, polynomial, exponential and B-spline functions have been proposed to model the behaviour of semi-rigid connections with reasonable accuracy (Richard and Abbott 1975, Kishi and Chen 1990, Attiogbe and Morris 1991).

Since in the formulation presented in this study the element nodal forces are primary unknowns, using a behavioural model which explicitly expresses the generalised displacement of the spring $q$ in terms of the generalised force $f$ can facilitate the computer implementation of the model. In this study, the widely-known Ramberg-Osgood model which originally proposed by Ramberg and Osgood (1943) and then standardised by Ang and Morris (1984) is adopted and for the unloading/reloading branch Masing's rule is employed which leads to an independent hardening model (Fig. 4(a)).

Using the total secant concept and decomposing the total generalised displacement $q$ to elastic $q_e$ and plastic $q_p$ components, the generalised force-displacement relationship for nodal springs can be expressed by

$$f = k(q - q_p), \tag{14}$$

where $f$ is the generalised force and $k$ is the elastic secant modulus of the unloading curve (Fig. 4b).

With regard to Fig. 1(b) and Eq. (14), the generalised load-displacement relationships of the nodal springs is condensed into matrix form as

$$\overline{\mathbf{q}} - \overline{\mathbf{q}}' = \mathbf{F}_{sp}\,\overline{\mathbf{Q}} + \overline{\mathbf{q}}_{p_r}\,, \tag{15}$$

where $\overline{\mathbf{q}} = [\overline{q}_1 \quad \overline{q}_2 \quad \overline{q}_3]^T$ and $\overline{\mathbf{Q}} = [\overline{Q}_1 \quad \overline{Q}_2 \quad \overline{Q}_3]^T$ are the generalised nodal deformation and force vectors of the frame element including nodal springs (without rigid body modes) respectively, $\overline{\mathbf{q}}_{p_r} = [q_{p1} + q_{p2} \quad q_{\theta_{p1}} \quad q_{\theta_{p2}}]^T$ is the generalised plastic deformation vector of the nodal spring system and $\mathbf{F}_{sp}$ represents the flexibility matrix of the nodal springs system given by

$$\mathbf{F}_{sp} = \begin{bmatrix} \dfrac{1}{k_1} + \dfrac{1}{k_2} & 0 & 0 \\ 0 & \dfrac{1}{k_{\theta 1}} & 0 \\ 0 & 0 & \dfrac{1}{k_{\theta 2}} \end{bmatrix}. \tag{16}$$

Substituting $\overline{\mathbf{q}}'$ from Eq. (10) into Eq. (15) produces

$$\overline{\mathbf{q}} = (\mathbf{F} + \mathbf{F}_{sp})\overline{\mathbf{Q}} + (\overline{q}_p + \overline{q}_p,) + \overline{q}_{und.}\,. \tag{17}$$

It is noteworthy that in the proposed total secant approach the material stiffness as well as the stiffness of semi-rigid connections (i.e., nodal springs) are always positive regardless the material/spring is hardening or softening. Accordingly, the stiffness matrices of the frame element as well as the spring system remain positive definite at all stages of analysis and does not become ill-conditioned.

## 3. Displacement interpolation along the element axis

In regard to Eq. (5), it is observed that incorporating the geometrical nonlinearity into the flexibility formulation necessitates the deformed shape of the element to be known. In the displacement-based formulation, the deformed shape of the element can be obtained based on the nodal displacement values and adopted shape functions. In the force-based element, however, there is no displacement shape function that can be used and a different technique is required (Carol and Murcia 1989b, Valipour and Foster 2010b).

Adopting the small strains and slopes implicit within routine Euler beam theory leads to the displacement-strain relationships for an arbitrary section at $x$ along the element (Fig. 2) given by

$$v(x) = q_2 + x\,q_3 + \int_0^x (x-s)\,\kappa(s)\,\mathrm{d}s\,, \tag{18}$$

where $v(x)$ is the lateral displacement of the section at $x$. With regard to Fig. 2, the undulation deflection $v'(x)$ is calculated as

$$v'(x) = \left\{\frac{(q_5 - q_2)}{l} - q_3\right\} x - \int_0^x (x-s)\,\kappa(s)\,\mathrm{d}s\,. \tag{19}$$

Following the approach devised by Valipour (2009), in this study a composite Simpson integration method together with piecewise parabolic interpolation of the curvature is used to update the element geometry.

## 4. Rigid body motion and corresponding transformation

If the length of the nodal springs is taken to be negligible compared to that of the member, the transformation between the force vectors of the systems with and without rigid body modes can be established as

$$\mathbf{Q} = \mathbf{T}^T\,\overline{\mathbf{Q}} + \mathbf{Q}_{P-\Delta}\,, \tag{20}$$

where $\mathbf{Q} = [Q_1 \quad Q_2 \quad Q_3 \quad Q_4 \quad Q_5 \quad Q_6]^T$ denotes the vector of the nodal forces in the system with rigid body modes, $T$ is the transformation matrix given by

$$\mathbf{T} = \left[\begin{array}{ccc:ccc} 1 & 0 & 0 & -1 & 0 & 0 \\ 0 & 1/l & 1 & 0 & -1/l & 0 \\ 0 & 1/l & 0 & 0 & -1/l & 1 \end{array}\right] \tag{21}$$

and $\mathbf{Q}_{P-\Delta}$ is a vector of nodal forces due to the $P-\Delta$ effect and is calculated as

$$\mathbf{Q}_{P-\Delta} = [0 \quad Q_1(q_5 - q_2)/l \quad 0 \quad 0 \quad Q_1(q_2 - q_5)/l \quad 0]^T\,. \tag{22}$$

Assuming that the element rotation is negligible compared to unity, the geometric compatibility equation is obtained as

$$\overline{\mathbf{q}} = \mathbf{T}\,\mathbf{q}\,, \tag{23}$$

where $\mathbf{q} = [q_1 \quad q_2 \quad q_3 \quad q_4 \quad q_5 \quad q_6]^T$ denotes the nodal displacement vector in the system with rigid body modes.

If the stiffness matrix of the simply supported configuration including the nodal springs (without rigid body modes) is denoted by $\mathbf{K} = \{\mathbf{F} + \mathbf{F}_{sp}\}^{-1}$, then Eq. (17) can be rewritten as

$$\overline{\mathbf{Q}} = \mathbf{K}\left\{\overline{\mathbf{q}} - (\overline{\mathbf{q}}_p + \overline{\mathbf{q}}_{p_r}) - \overline{\mathbf{q}}_{und.}\right\}. \tag{24}$$

Multiplying Eq. (24) by $\mathbf{T}^T$ and then substituting for $\overline{\mathbf{q}}$ from Eq. (23) results in

$$\left\{\mathbf{T}^T\mathbf{K}\mathbf{T}\right\}\mathbf{q} = \mathbf{Q} + \mathbf{T}^T\mathbf{K}(\overline{\mathbf{q}}_p + \overline{\mathbf{q}}_{p_r}) + (\mathbf{T}^T\mathbf{K}\overline{\mathbf{q}}_{und.} - \mathbf{Q}_{P-\Delta}). \tag{25}$$

The recursive form of Eq. (25) which can be solved for static loads by following a direct iterative solution scheme (Valipour and Foster 2010a) after assembling at the structure level is

$${}^{(i-1)}\mathbf{K}_{St.}\ {}^{(i)}\mathbf{q}_{St.} = \mathbf{R}_{St.} + {}^{(i-1)}\mathbf{F}_{St.}, \tag{26}$$

where ${}^{(i-1)}\mathbf{K}_{St.} = \sum_{\text{elem=1}}^{n}\left\{{}^{(i-1)}\mathbf{T}^T\ {}^{(i-1)}\mathbf{K}\ {}^{(i-1)}\mathbf{T}\right\}$ is the assembled stiffness matrix of the structure, $\mathbf{R}_{St.}$ is the external nodal force vector, the left superscript ($i$-1) denotes the iteration number and ${}^{(i-1)}\mathbf{F}_{St.}$ is

$${}^{(i-1)}\mathbf{F}_{St.} = \sum_{\text{elem=1}}^{n}{}^{(i-1)}\mathbf{T}^T\ {}^{(i-1)}\mathbf{K}\left({}^{(i-1)}\overline{\mathbf{q}}_p + {}^{(i-1)}\overline{\mathbf{q}}_{p_r}\right) + \sum_{\text{elem=1}}^{n}\left({}^{(i-1)}\mathbf{T}^T\ {}^{(i-1)}\mathbf{K}\ {}^{(i-1)}\overline{\mathbf{q}}_{und.} - {}^{(i-1)}\mathbf{Q}_{P-\Delta}\right). \tag{27}$$

Additionally, the recursive form of the dynamic equilibrium equations for a discretised system at the instant $t+\Delta t$ is

$$\mathbf{M}_{St.}\ {}^{(i)}\ddot{\mathbf{q}}_{St.}^{t+\Delta t} + \mathbf{C}_{St.}\ {}^{(i)}\dot{\mathbf{q}}_{St.}^{t+\Delta t} + {}^{(i-1)}\mathbf{K}_{St.}\ {}^{(i)}\mathbf{q}_{St.}^{t+\Delta t} = \mathbf{R}_{St.}^{t+\Delta t} + {}^{(i-1)}\mathbf{F}_{St.}, \tag{28}$$

where $\mathbf{M}_{St.}$ and $\mathbf{C}_{St.}$ are the mass and damping matrices of the structure, and ${}^{(i)}\mathbf{q}_{St.}^{t+\Delta t}$, ${}^{(i)}\dot{\mathbf{q}}_{St.}^{t+\Delta t}$ and ${}^{(i)}\ddot{\mathbf{q}}_{St.}^{t+\Delta t}$ denote displacement, velocity and acceleration vectors of the structure, respectively. After the time discretisation of the differential equation (28) by employing a standard method such as the Newmark or $\theta$-Wilson method (Bathe 1997), the recursive equations can be solved by following a direct iterative scheme (Valipour and Foster 2010a).

In the numerical examples presented in this paper, wherever required, a proportional damping in the form of $\mathbf{C}_{St.} = \alpha\mathbf{M}_{St.} + \beta\mathbf{K}_{St.}$ is adopted.

## 5. Inclusion of shear springs in the model

The nodal shear (transverse) springs can be easily incorporated into the developed formulation using equilibrium and displacement compatibility equations of the compound element shown in Fig. 5(a).

Using the total secant concept and decomposing the total generalised displacement to elastic and plastic components, the generalised force-displacement relationship for shear springs $k_{s1}$ and $k_{s2}$ attached to the nodal points (see Fig. 5(b)) can be expressed by

$$Q_2 = k_{s1}\left(q_2 - q_2' - q_{p2}\right) \quad \text{and} \tag{29a}$$

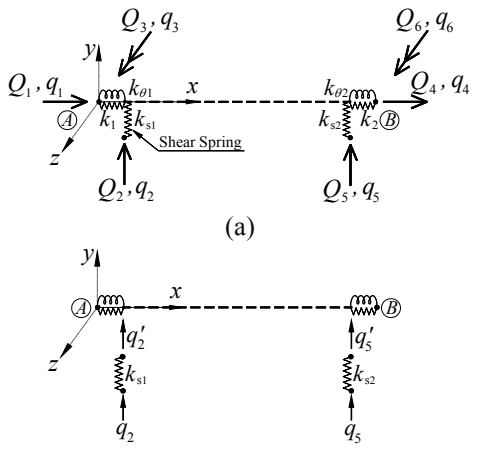


Fig. 5 Outline of the (a) compound element *AB* with axial, rotational and shear springs (b) transverse nodal degrees of freedom corresponding to shear springs

$$Q_5 = k_{s2}\left(q_5 - q_5' - q_{p5}\right). \tag{29b}$$

For the compound element with shear springs (see Fig. 5(b)), Eq. (25) can be rewritten as

$$\mathbf{q}' = \left\{\mathbf{T}^T\mathbf{K}\mathbf{T}\right\}^{-1}\left(\mathbf{Q} - \mathbf{Q}'_{P-\Delta}\right) + \mathbf{T}^{-1}\left(\overline{\mathbf{q}}_p + \overline{\mathbf{q}}_{p_r} + \overline{\mathbf{q}}_{und.}\right), \tag{30}$$

where $\mathbf{q}' = \begin{bmatrix} q_1 & q_2' & q_3 & q_4 & q_5' & q_6 \end{bmatrix}^T$ and

$$\mathbf{Q}_{P-\Delta} = \begin{bmatrix} 0 & Q_1(q_5' - q_2')/l & 0 & 0 & Q_1(q_2' - q_5')/l & 0 \end{bmatrix}^T. \tag{31}$$

Taking $q_2'$ and $q_5'$ from Eq. (29) and submitting it into $q'$ on the left-side of Eq. (30) produces

$$\mathbf{q} = \left\{\mathbf{T}^T\mathbf{K}\mathbf{T}\right\}^{-1}\left(\mathbf{Q} - \mathbf{Q}'_{P-\Delta}\right) + \mathbf{T}^{-1}\left(\overline{\mathbf{q}}_p + \overline{\mathbf{q}}_{p_r} + \overline{\mathbf{q}}_{und.}\right) + \mathbf{F}_s\,\mathbf{Q} + \mathbf{q}_{p_s}, \tag{32}$$

where

$$\mathbf{F}_s = \begin{bmatrix} 0 & 0 & 0 & 0 & 0 & 0 \\ 0 & 1/k_{s1} & 0 & 0 & 0 & 0 \\ 0 & 0 & 0 & 0 & 0 & 0 \\ 0 & 0 & 0 & 0 & 0 & 0 \\ 0 & 0 & 0 & 0 & 1/k_{s2} & 0 \\ 0 & 0 & 0 & 0 & 0 & 0 \end{bmatrix}, \tag{33}$$

is the flexibility matrix of the nodal shear springs and

$$\mathbf{q}_{p_s} = \begin{bmatrix} 0 & q_{p2} & 0 & 0 & q_{p5} & 0 \end{bmatrix}^T, \tag{34}$$

is the generalised plastic deformation vector of the nodal shear springs.

Eq. (32) can be recast into the following matrix form which is more suitable for finite element implementation,

$$\begin{aligned}\left\{\left[\mathbf{T}^T\mathbf{K}\mathbf{T}\right]^{-1}+\mathbf{F}_s\right\}^{-1}\mathbf{q}=&\mathbf{Q}-\left\{\mathbf{I}+\left[\mathbf{T}^T\mathbf{K}\mathbf{T}\right]\mathbf{F}_s\right\}^{-1}\mathbf{Q}'_{P-\Delta}\\+\left\{\left[\mathbf{T}^T\mathbf{K}\mathbf{T}\right]^{-1}+\mathbf{F}_s\right\}^{-1}&\mathbf{q}_{p_s}+\left\{\left[\mathbf{T}^T\mathbf{K}\right]^{-1}+\mathbf{T}\mathbf{F}_s\right\}^{-1}\left(\overline{\mathbf{q}}_p+\overline{\mathbf{q}}_{p_r}+\overline{\mathbf{q}}_{und.}\right)\end{aligned}. \tag{35}$$

The recursive form of Eq. (35) can be solved by following a direct iterative solution scheme (Valipour and Foster 2010a) as described in previous section.

The proposed model can only capture the axial, shear and flexural deformation of connections and the formulation is only applicable when effect of torsion and torsional behaviour of semi-rigid connection are not significant.

## 6. Numerical examples

### *6.1 P-Δ analysis of a column with flexible end connections*

This first example is used to demonstrate the performance of the developed formulation for the *P*-Δ analysis of a linear-elastic column with flexible end connections, and the results are compared with more demanding displacement-based formulation using cubic Hermitian shape functions. The geometry of the column, boundary conditions and loading are shown in Fig. 6. The elastic modulus of material is $E=200\,\text{GPa}$ and the shear deformation is ignored. It is noteworthy that the developed formulation can capture both material and geometrical nonlinearities, however, in this example the concentration is only on the geometrical *P*-Δ effects and accordingly the column is assumed to be linear-elastic.

The values of lateral displacement at end *B* obtained from force-based formulation developed in this paper, as well as the results of a displacement-based method for different levels of load *P*, are shown in Table 1. Using a displacement-based model, at least 8 to 16 elements are required to obtain a degree of accuracy comparable to a single flexibility element using a 7-point Simpson

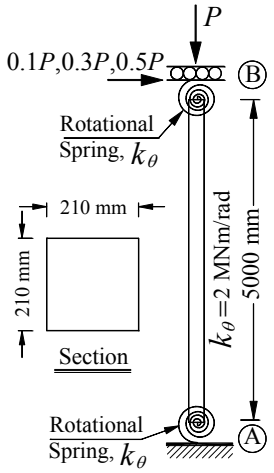


Fig. 6 Geometry of the column, boundary conditions and loading

Table 1 Lateral displacement at point *B* at different levels of load *P* obtained from flexibility and displacement-based formulations with different number of element or integration points (Int. pts.)

| | | Lateral displacement at point *B* (mm) | | | | | | | |
|---|---|---|---|---|---|---|---|---|---|
| | | Cubic Hermitian shape function | | | | Present study (1 element) | | | |
| Lateral load | No. of element (No. Int. pts.) | 1 | 2 | 4 | 8 | 16 | 64 | 5 pts | 9 pts |
| 0.1P | P= 100 kN | 77.7 | 77.2 | 76.4 | 76.0 | 75.7 | 75.5 | 75.4 | 75.3 |
| | P= 200kN | 191.4 | 187.3 | 182.5 | 180.1 | 179.1 | 178.1 | 176.9 | 176.6 |
| | P= 300 kN | 373.2 | 356.8 | 339.8 | 332.1 | 328.3 | 325.1 | 321.6 | 319.8 |
| 0.3P | P= 100 kN | 233.9 | 231.7 | 229.2 | 228.0 | 227.4 | 226.6 | 224.5 | 223.9 |
| | P= 200kN | 574.2 | 561.8 | 547.4 | 540.8 | 537.2 | 535.0 | 529.8 | 528.5 |
| | P= 300 kN | 1119.7 | 1070.5 | 1019.4 | 996.4 | 985.0 | 977.6 | 963.4 | 959.2 |
| 0.5P | P= 100 kN | 389.8 | 386.1 | 381.9 | 380.0 | 379.1 | 377.7 | 373.2 | 372.7 |
| | P= 200kN | 956.9 | 936.4 | 912.3 | 901.4 | 895.3 | 891.7 | 883.9 | 881.3 |
| | P= 300 kN | 1866.2 | 1784.2 | 1699. | 1660.6 | 1641.6 | 1629.4 | 1598.7 | 1589.1 |

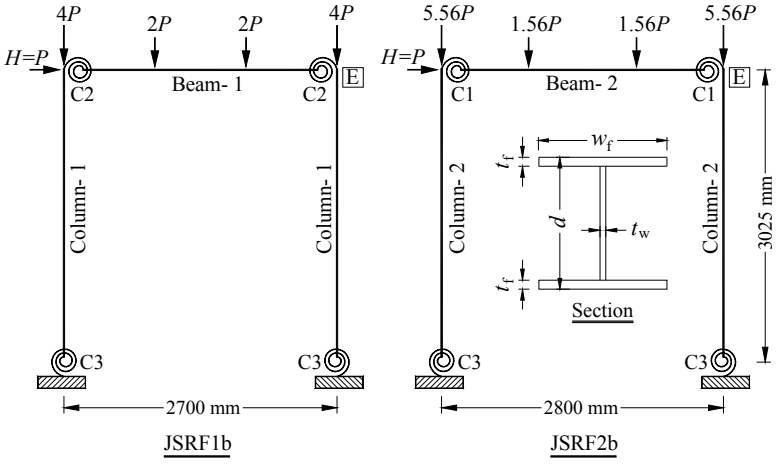


| Section | $w_f$ (mm) | $t_f$ (mm) | $d$ (mm) | $t_w$ (mm) | $\sigma_y$ (MPa) |
|---|---|---|---|---|---|
| Column-1 | 208.8 | 20.5 | 222.3 | 13.0 | 318 |
| Beam-1 | 172.1 | 13.0 | 358.6 | 8.0 | 303 |
| Column-2 | 205.2 | 14.2 | 210.0 | 9.3 | 336 |
| Beam-2 | 146.4 | 10.9 | 256.0 | 6.4 | 345 |

Steel elastic modulus: $E_s$ = 200 (GPa)
Steel yield stress: $\sigma_y$

Fig. 7 Geometry of members and sections, details of loadings and material properties for frames JSRF1b and JSRF2b tested by Liew *et al*. (1997)

integration scheme. This demonstrates the superior efficiency and accuracy of the formulation presented in this study.

### *6.2 Static analysis of a portal frame*

In this example, one-storey one-bay portal frames JSRF1b and JSRF2b, tested by (Liew *et al*. 1997) are analysed. The geometry of the specimens, details of loading and material properties are given in Fig. 7. In addition, by applying a curve fitting technique, the moment-rotation response of

the semi-rigid connections C1, C2 and C3 are obtained based on the Ang and Morris (1984) three-parameter model and are compared with the experimental moment-rotation curves in Fig. 8.

Using the force-based compound-element developed in this study, the frame was modelled with 3 elements: one for each member (i.e., beam and column) of the frame. The FE model of the frame within the force-based formulation has 6 DOFs corresponding to 2 unrestrained nodes. The integrals are estimated by a composite Simpson's integration scheme with 15 integration points through the section depth (3 points over the thickness of each flange) and 11 points along the members.

The lateral load $H$ versus the drift of the storey at point $E$ obtained from the developed formulation, together with the experimental results and the results of a refined-plastic-hinge formulation from Chen *et al.* (1996) are shown in Fig. 9. It can be observed that the numerical results correlate reasonably well with the experimental ones and the present formulation has the capability to capture the global response as well as the ultimate loading capacity of the semi-rigid frames with reasonable accuracy. The discrepancy between the experimental and numerical results can be attributed to the connection behaviour data determined by separate pilot experiments which were somewhat different from the behaviour of the connections in the actual frame itself.

The results obtained from the force-based compound-element with and without second order $P$-$\Delta$ effects for different numbers of longitudinal integration points are shown in Fig. 10. With regard to this figure, it can be observed that the formulation including second order $P$-$\Delta$ effects captures the response more accurately whereas the first order analysis overestimates the loading

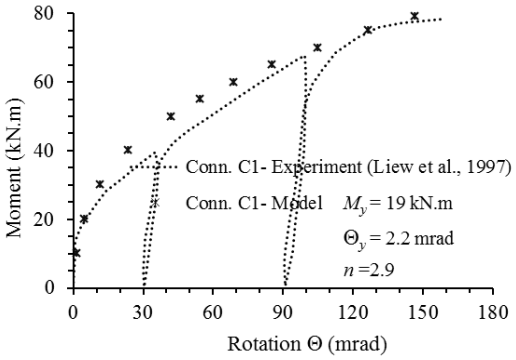


(a) Connection C1

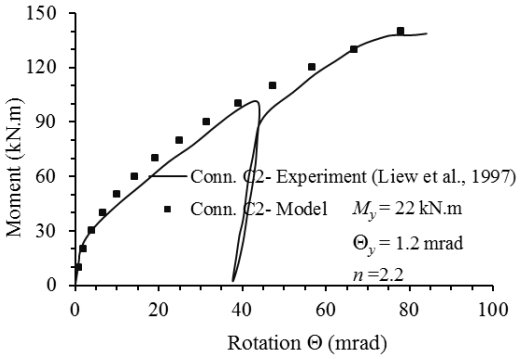


(b) Connection C2

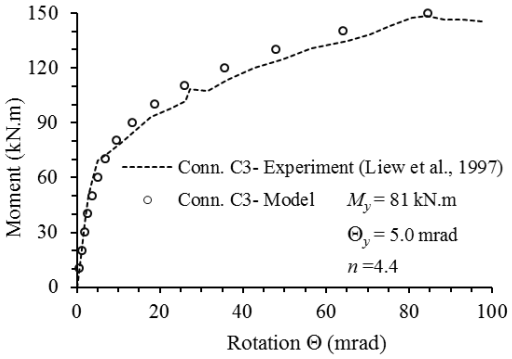


(c) Connection C3

Fig. 8 Moment-rotation relationship for semi-rigid connections

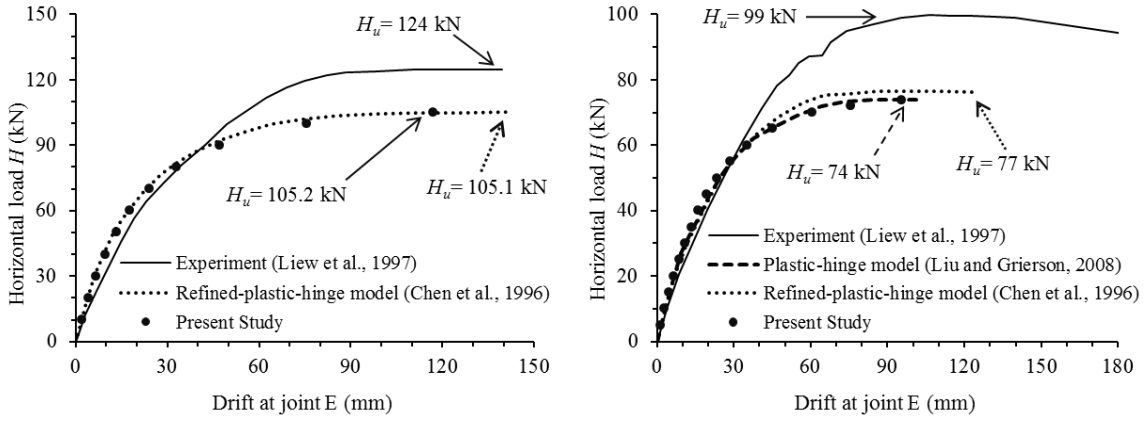


Fig. 9 Lateral load $H$ versus drift at point E for specimen (a) JSRF1b (b) JSRF2b

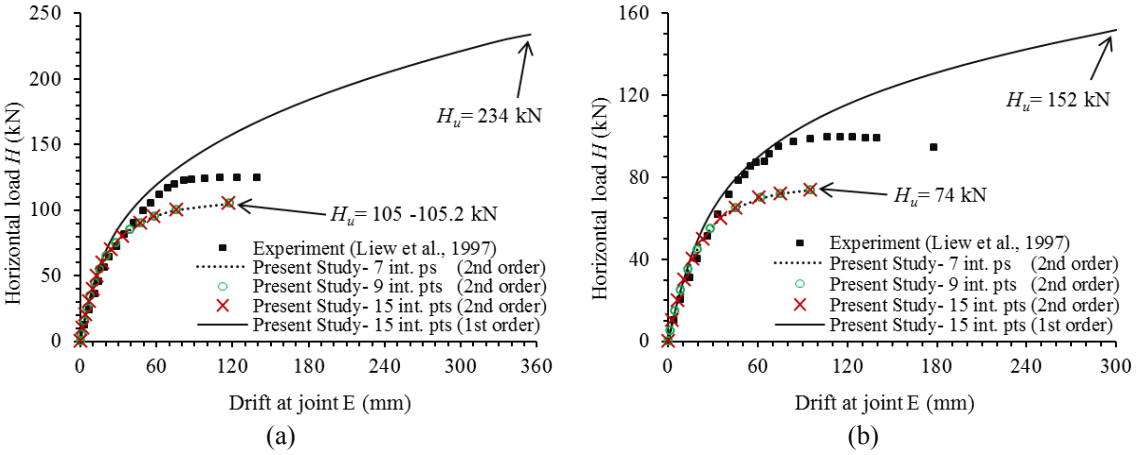


Fig. 10 Lateral load $H$ versus drift at point E for specimen (a) JSRF1b (b) JSRF2b obtained from force-based compound-element with and without second order $P$-Δ effects included

capacity of the structure. The difference between the two formulations (i.e., with and without geometric nonlinearity) becomes more pronounced at ultimate stages of loading. Furthermore, Fig. 10 shows that the results are not sensitive to number of longitudinal integration points and even an integration scheme with 7 points along the element axis can capture the geometrically and materially nonlinear response of the member reasonably well. Using more than 9 integration points along the element axis does not improve the results and it merely increases the computational cost.

### *6.3 Two-storey frame subjected to cyclic lateral load*

In this example, the two-storey frame tested by Stelmack *et al*. (1986) is analysed. The geometry of frame and sections, loading and the material properties are given in Fig. 11. Further, the history of cyclic loading and the experimental and analytical moment-rotation response of the connections are shown in Fig. 12.

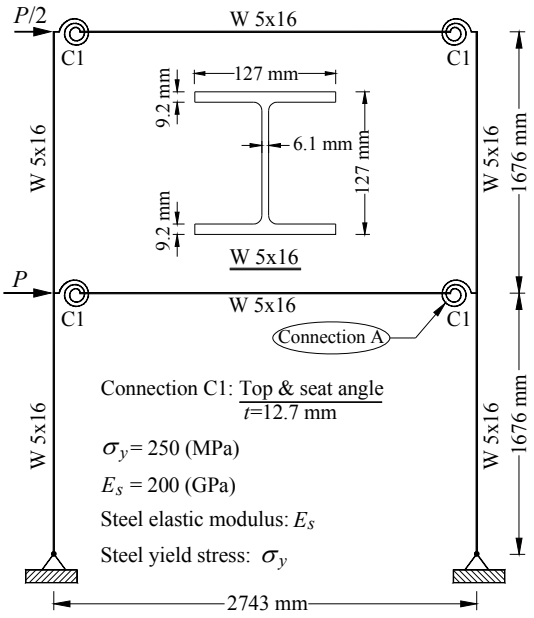


Fig. 11 Geometry of members and sections, details of loading and material properties for frame tested by Stelmack (1986)

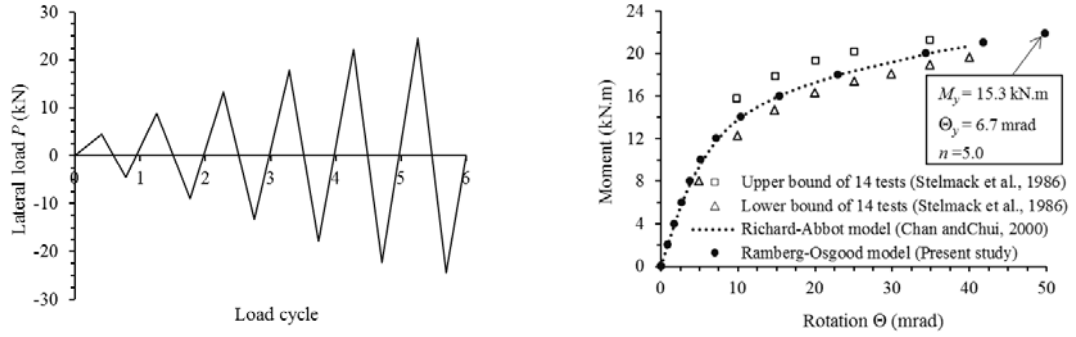


(a) (b)

Fig. 12 (a) History of the cyclic loading and (b) moment-rotation relationship of the connections for the semi-rigid frame tested by Stelmack (1986)

Using the force-based formulation developed in this study, the frame was modelled with 6 elements: one for each member (i.e., beam and column) of the frame. The integrals are estimated by a composite Simpson's integration scheme with 15 integration points through the section depth (3 points over the thickness of each flange), 11 integration points along the beams and 9 points along the columns.

The lateral load $P$ versus the drift at the first and second storey and moment-rotation response of connection A for different cycles are shown in Figs. 13 to 15, respectively. It can be observed that the displacement and force responses obtained from analysis correlate reasonably well with the experimental data. The discrepancy between numerical predictions and experimental results can be attributed to the behavioural model adopted for steel and semi-rigid connections. In

particular, the loading/unloading model adopted for connections can affect the local as well as the global response of the structure subject to the cyclic loads. Furthermore, at later stages of loading when plastic hinges start to form the response of structure is influenced by hardening modulus of steel which is not available from the experiment.

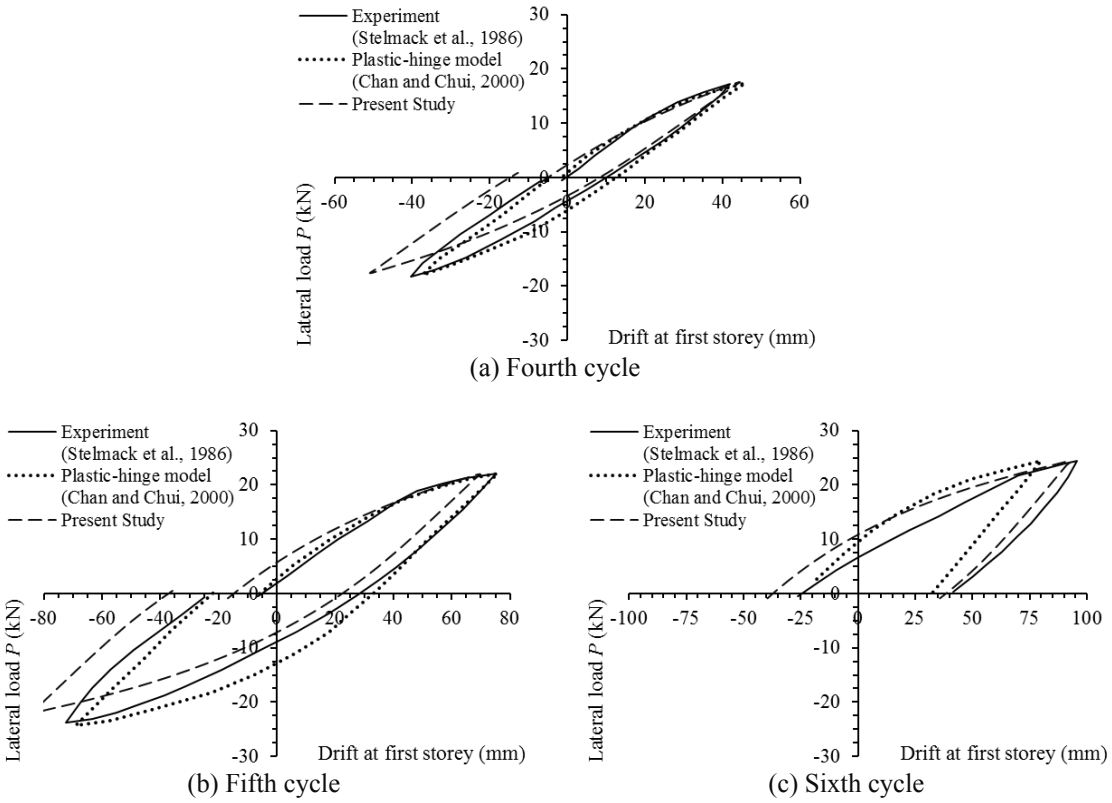


(a) Fourth cycle

(b) Fifth cycle

(c) Sixth cycle

Fig. 13 Lateral load *P* versus drift for first storey at different cycles

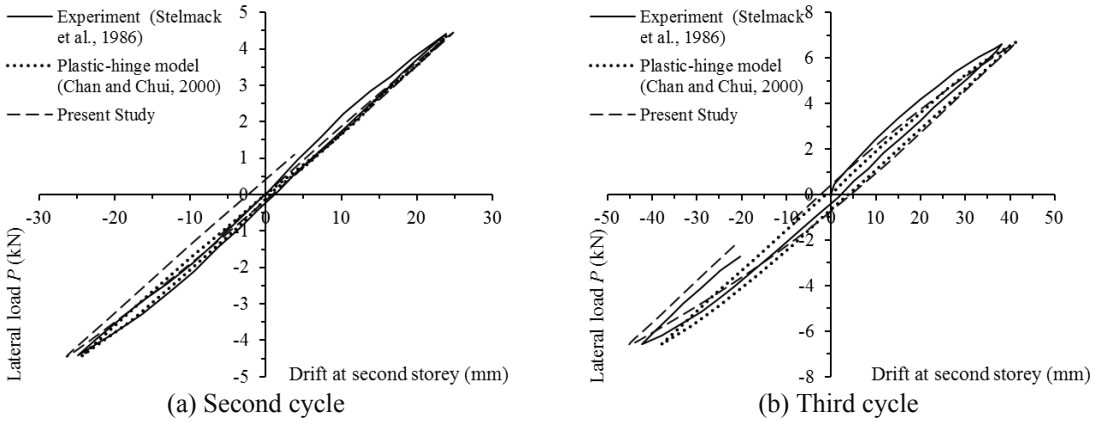


(a) Second cycle

(b) Third cycle

Fig. 14 Lateral load *P* versus drift for second storey at different cycles

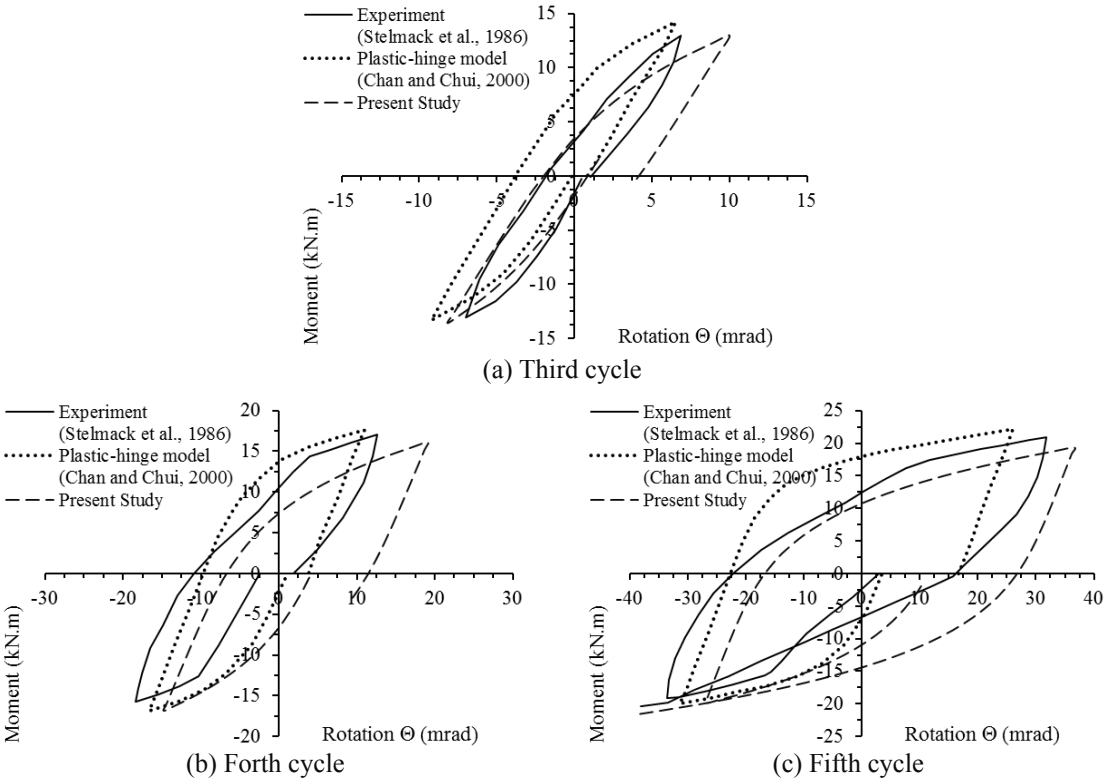


(a) Third cycle

(b) Forth cycle

(c) Fifth cycle

Fig. 15 Moment-rotation response of connection *A* at different cycles

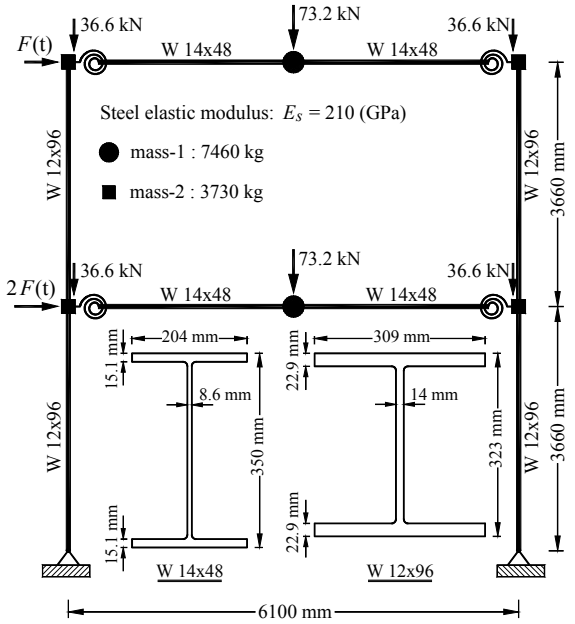


Fig. 16 Geometry of members and sections, details of loading and material properties for unbraced two-storey frame

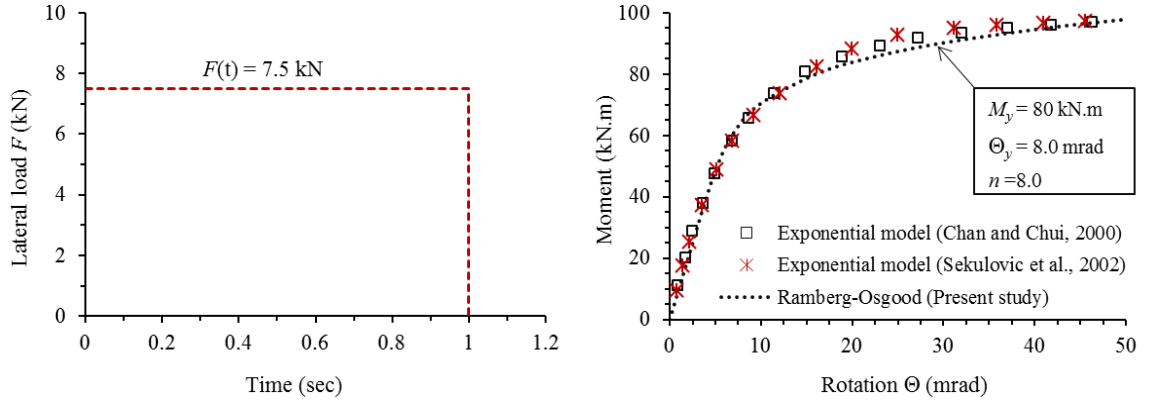


(a) (b)

Fig. 17 (a) History of the dynamic loading and (b) moment-rotation relationship for the semi-rigid connections

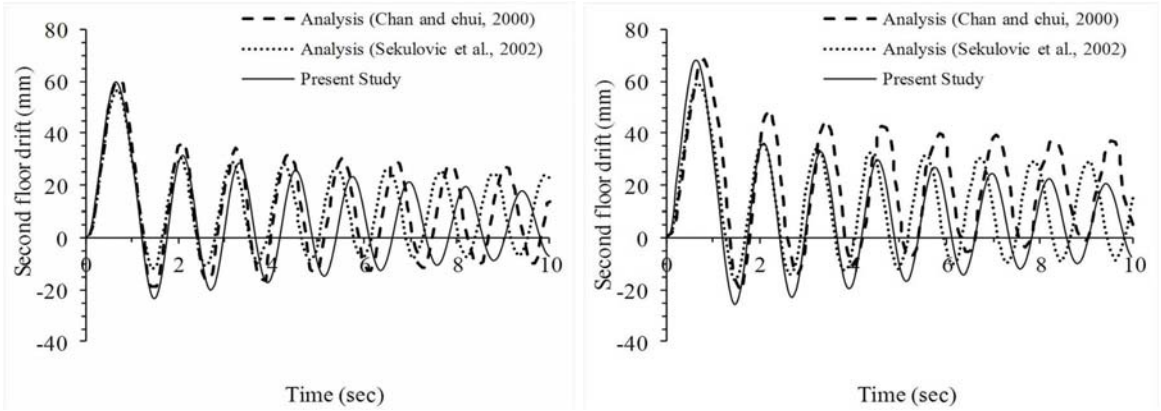


(a) (b)

Fig. 18 History of second floor drift for the case (a) without gravity loads (b) with gravity loads

### *6.4 Dynamic analysis of frame with nonlinear connections*

In this example, the transient response of a one-bay two-storey frame whose geometry and loading are shown in Fig. 16 for cases with and without gravity loads is studied, and the results are compared with response obtained by Sekulovic *et al*. (2002) and Chan and Chui (2000). Furthermore, the history of the lateral load and the analytical moment-rotation relationship for connections adopted in this study are shown in Figs. 17(a) and 17(b) respectively. It is assumed that all of the frame elements except connections remain elastic.

Using force-based elements developed in this study, the entire frame was modelled by 8 elements (two elements per beam and one element per column). The integrals are estimated by a composite Simpson's integration scheme with 15 integration points through the section depth (3 points over thickness of each flange) and the distance between longitudinal integration points is limited to 300 mm.

The Newmark scheme with a time step of 0.05 sec was used for the dynamic analysis. In addition, a Rayleigh damping proportional to the mass matrix with a multiplier of $\alpha = 0.2$ was

adopted for dynamic analysis. The history of the second floor drift for cases without and with gravity load is shown in Fig. 18, which shows reasonable correlation with the analytical results obtained by Sekulovic *et al*. (2002) and Chan and Chui (2000). For the case without gravity load, the maximum drift of second floor predicted by the developed formulation is $\delta_{max}$ = 59.9 mm which correlates very well with $\delta_{max}$ = 60.4 mm obtained from Chan and Chui (2000) analysis and slightly more than $\delta_{max}$ = 56.6 mm predicted in Sekulovic *et al*. (2002). Concerning the case with gravity load, the developed formulation gives $\delta_{max}$ = 67.9 mm deflection compared to $\delta_{max}$ = 68.4 mm predicted by Chan and Chui (2000) analysis. The difference between responses, particularly at later stages of time history, can be attributed to level of damping and loading/unloading model adopted for connections.

## 7. Conclusions

A novel force-based formulation in the framework of the total secant stiffness matrix has been derived for 1-D frame elements with flexible end connections. The formulation takes account of material and geometrical nonlinearities as well as the nonlinearity of the end connections within small strain/slope theory of beams. A composite Simpson integration scheme with a piecewise parabolic interpolation of curvature was used to calculate the displacement of the sections along the element axis required for the $P$-$\Delta$ geometrical nonlinearities associated with undulation effect. The formulation accuracy and efficiency established by comparisons with available methods, being verified by four numerical examples, and it was shown that by using only one element per member (i.e., beam or column) the formulation has the capability to capture the global response of semi-rigid frames with very high accuracy.

## References

Ang, K.M. and Morris, G.A. (1984), "Analysis of three-dimensional frames with flexible beam-column connections", *Canadian J. Civil Eng*., **11**(2), 245-254.

Ashraf, M., Nethercot, D.A. and Ahmed, B. (2004), "Sway of semi-rigid steel frames Part 1: Regular frames", *Eng. Struct*., **26**(12), 1809-1819.

Attiogbe, E. and Morris, G. (1991), "Moment-rotation functions for steel connections", *J. Struct. Eng*., *ASCE*, **117**(6), 1703-1718.

Bathe, J.K. (1997), *Finite element procedures*, New York, McGraw Hill.

Bayo, E., Cabrero, J.M. and Gil, B. (2006), "An effective component-based method to model semi-rigid connections for the global analysis of steel and composite structures", *Eng. Struct*., **28**(1), 97-108.

Carol, I. and Murcia, J. (1989a), "Nonlinear time-dependent analysis of planar frames using an 'exact' formulation. I. Theory", *Comput. Struct*., **33**(1), 79-87.

Carol, I. and Murcia, J. (1989b), "Nonlinear time-dependent analysis of planar frames using an 'exact' formulation. II. Computer implementation for R.C. structures and examples", *Comput. Struct*., **33**(1), 89-102.

Chan, S.L. and Cho, S.H. (2008), "Second-order analysis and design of angle trusses Part I: Elastic analysis and design", *Eng. Struct*., **30**(3), 616-625.

Chan, S.L. and Chui, P.P.T. (2000), *Non-linear static and cyclic analysis of steel frames with semi-rigid connections*, Amsterdam, Elsevier.

Chen, W.F., Goto, Y. and Liew, J.Y.R. (1996), *Stability design of semi-rigid frames*, New York, John Wiley & Sons, Inc.

Chen, W.F. and Kishi, N. (1989), "Semi-rigid steel beam-to-column connections: Data base and modeling", *J. Struct. Eng., ASCE*, **115**(1), 105-119.
Cheng, F.Y. and Juang, D.S. (1986), "Effects of P-Delta and semi-rigid connections on response behaviour of inelastic steel frames subjected to cyclic and siesmic loadings", *ASCE*, 32-50.
Chiorean, C.G. (2009), "A computer method for nonlinear inelastic analysis of 3D semi-rigid steel frameworks", *Eng. Struct.*, **31**(12), 3016-3033.
Chui, P.P.T. and Chan, S.L. (1996), "Transient response of moment-resistant steel frames with flexible and hysteretic joints". *J. Constr. Steel Res.*, **39**(3), 221-243.
Da S. Vellasco, P.C.G., De Andrade, S.a.L., Da Silva, J.G.S., De Lima, L.R.O. and Brito Jr., O. (2006), "A parametric analysis of steel and composite portal frames with semi-rigid connections", *Eng. Struct.*, **28**(4), 543-556.
Da Silva, J.G.S., De Lima, L.R.O., Da S. Vellasco, P.C.G., De Andrade, S.a.L. and De Castro, R.A. (2008), "Nonlinear dynamic analysis of steel portal frames with semi-rigid connections", *Eng. Struct.*, **30**(9), 2566-2579.
De Lima, L.R.O., Freire, J.L.D.F., Vellasco, P.C.G.D.S., Andrade, S.a.L.D. and Silva, J.G.S.D. (2009), "Structural assessment of minor axis steel joints using photoelasticity and finite elements", *J. Constr. Steel Res.*, **65**(2), 466-478.
Ding, J. and Wang, Y.C. (2009), "Temperatures in unprotected joints between steel beams and concrete-filled tubular columns in fire", *Fire Safety J.*, **44**(1), 16-32.
Hadianfard, M.A. (2012), "Using integrated displacement method to time-history analysis of steel frames with nonlinear flexible connections", *Struct. Eng. Mech.*, **41**(5), 675-689.
Han, L.H., Huo, J.S. and Wang, Y.C. (2007), "Behavior of steel beam to concrete-filled steel tubular column connections after exposure to fire", *J. Struct. Eng., ASCE*, **133**(6), 800-814.
Iu, C.K., Bradford, M.A. and Chen, W.F. (2009), "Second-order inelastic analysis of composite framed structures based on the refined plastic hinge method", *Eng. Struct.*, **31**(3), 799-813.
Iu, C.K., Chan, S.L. and Zha, X.X. (2007), "Material yielding by both axial and bending spring stiffness at elevated temperature", *J. Constr. Steel Res.*, **63**(5), 677-685.
Ivanyi, M. (2000), "Full-scale tests of steel frames with semi-rigid connections", *Eng. Struct.*, **22**(2), 168-179.
Khandelwal, K., El-Tawil, S., Kunnath, S.K. and Lew, H.S. (2008), "Macromodel-based simulation of progressive collapse: Steel frame structures". *J. Struct. Eng.,* **134**(7), 1070-1078.
Kishi, N. and Chen, W.F. (1990), "Moment-rotation relations of semirigid connections with angles", *J. Struct. Eng., ASCE*, **116**(7), 1813-1834.
Kukreti, A.R. and Abolmaali, A. (1999), "Moment-rotation hysteresis behavior of top and seat angle steel frame connections", *ASCE, J. Struct. Eng.*, **125**(8), 810-820.
Liew, J.Y.R., Yu, C.H., Ng, Y.H. and Shanmugam, N.E. (1997), "Testing of semi-rigid unbraced frames for calibration of second-order inelastic analysis", *J. Constr. Steel Res.*, **41**(2-3), 159-195.
Liu, Y., Xu, L. and Grierson, D.E. (2008), "Compound-element modeling accounting for semi-rigid connections and member plasticity", *Eng. Struct.*, **30**(5), 1292-1307.
Mohamadi-Shooreh, M.R. and Mofid, M. (2008), "Parametric analyses on the initial stiffness of flush end-plate splice connections using FEM", *J. Constr. Steel Res.*, **64**(10), 1129-1141.
Prabha, P., Marimuthu, V., Arul Jayachandran, S., Seetharaman, S. and Raman, N. (2008), "An improved polynomial model for top -and seat- Angle connection", *Steel Compos. Struct.*, **8**(5), 403-421.
Ramberg, W. and Osgood, W.R. (1943), "Description of stress-strain curves by three parameters", *Report No. 902*, National Advisory Committee for Aeronautics, Washington, D.C.
Reyes-Salazar, A., Soto-Lópeza, M.E., Bojórquez-Morab, E. and López-Barrazab, A. (2012), "Effect of modeling assumptions on the seismic behavior of steel buildings with perimeter moment frames", *Struct. Eng. Mech.*, **41**(2), 183-204.
Richard, R.M. and Abbott, B.J. (1975), "Versatile elastic-plastic stress-strain formula", *ASCE, J. Engng. Mech.*, **101**(4), 511-515.
Rodrigues, F.C., Saldanha, A.C. and Pfeil, M.S. (1998), "Non-linear analysis of steel plane frames with

semi-rigid connections", *J. Constr. Steel Res.*, **46**(1-3), 94-97.
Saravanan, M., Arul Jayachandran, S., Marimuthu, V. and Prabha, P. (2009), "Advanced analysis of cyclic behaviour of plane steel frames with semi-rigid connections", *Steel Compos. Struct.*, **9**(4), 381-395.
Sekulovic, M. and Nefovska-Danilovic, M. (2008), "Contribution to transient analysis of inelastic steel frames with semi-rigid connections", *Eng. Struct.*, **30**(4), 976-989.
Sekulovic, M. and Salatic, R. (2001), "Nonlinear analysis of frames with flexible connections", *Comput. Struct.*, **79**(11), 1097-1107.
Sekulovic, M., Salatic, R. and Nefovska-Danilovic, M. (2002), "Dynamic analysis of steel frames with flexible connections", *Comput. Struct.*, **80**(9), 935-955.
Shen, J. and Astaneh-Asl, A. (1999), "Hysteretic behavior of bolted-angle connections", *J. Constr. Steel Res.*, **51**(3), 201-218.
Shi, G., Shi, Y., Wang, Y. and Bradford, M.A. (2008), "Numerical simulation of steel pretensioned bolted end-plate connections of different types and details", *Eng. Struct.*, **30**(10), 2677-2686.
Simoes Da Silva, L., De Lima, L.R.O., Da S. Vellasco, P.C.G. and De Andrade, S.a.L. (2004), "Behaviour of flush end-plate beam-to-column joints under bending and axial force", *Steel Compos. Struct.*, **4**(2), 77-94.
Spyrou, S., Davison, B., Burgess, I. and Plank, R. (2004), "Experimental and analytical studies of steel joint component at elevated temperatures", *Fire and Materials*, **28**(2-4), 83-94.
Stelmack, T.W., Marley, M.J. and Gerstle, K.H. (1986), "Analysis and tests of flexibly connected steel frames", *J. Struct. Eng., ASCE*, **112**(7), 1573-1588.
Trahair, N.S., Bradford, M.A., Nethercot, D.A. and Gardner, L. (2008), *The Behaviour and Design of Steel Structures to EC3,* London, Taylor and Francis.
Valipour, H.R. (2009), "Nonlinear analysis of reinforced concrete frames under extreme loadings, PhD Thesis", *PhD Dissertation*, *School of Civil and Environmental Engineering*, The University of New South Wales, Sydney, Australia,
Valipour, H.R. and Bradford, M. (2012), "An efficient compound-element for potential progressive collapse analysis of steel frames with semi-rigid connections", *Finite Elements in Analysis and Design*, **60**, 35-48.
Valipour, H.R. and Foster, S.J. (2010a), "Finite element modelling of reinforced concrete structures including catenary action", *Comput. Struct.,* **88**(9), 529-538.
Valipour, H.R. and Foster, S.J. (2010b), "A total secant flexibility-based formulation for frame elements with physical and geometrical nonlinearities". *Finite Elements in Analysis and Design*, **46**(3), 288-297.
Vu, A.Q. and Leon, R.T. (2008), "Vibration analysis of steel frames with semi-rigid connections on an elastic foundation", *Steel Compos. Struct.*, **8**(4), 265-280.
Wang, J.-F. and Li, G.-Q. (2007), "Testing of semi-rigid steel-concrete composite frames subjected to vertical loads", *Eng. Struct.*, **29**(8), 1903-1916.
Wang, J.-F. and Li, G.-Q. (2008), "A practical design method for semi-rigid composite frames under vertical loads", *J. Constr. Steel Res.*, **64**(2), 176-189.
Zarfam, P. and Mofid, M. (2009), "On the assessment of modal nonlinear pushover analysis for steel frames with semi-rigid connections", *Struct. Eng. Mech.*, **32**(3), 383-398.

*CC*